Journal of Materials Chemistry A

Accepted Manuscript

ROYAL SOCIETY OF CHEMISTRY

www.rsc.org/materialsA

Journal of Materials Chemistry A

Cite this: DOI: 10.1039/c0xx00000x

www.rsc.org/xxxxxx

ARTICLE TYPE

Electrochemical Properties and Morphological Evolution of Pitaya-like Sb@C Microspheres as High-performance Anode for Sodium Ion Batteries

*Lin Wu,[a] Haiyan Lu,[a] Lifen Xiao, *[b] Xinping Ai,[a] Hanxi Yang,[a] and Yuliang Cao *[a]*

Received (in XXX, XXX) Xth XXXXXXXXX 20XX, Accepted Xth XXXXXXXXX 20XX
DOI: 10.1039/b000000x

Pitaya-like Sb@C microspheres are prepared successfully by a facile aerosol spray drying synthesis. The structural and morphological characterizations reveal that the Sb@C microspheres present a uniform pitaya-like structure with well crystallized Sb nanoparticles embedded homogeneously in the carbon matrix. The Sb@C microsphere electrodes exhibit high Na storage capacity of 655 mAh g^{-1} at C/15 with excellent cyclability (93 % of capacity retention over 100 cycles) as well as remarkable rate capability. Also, the morphological evolution of the Sb@C microspheres is unravelled to account for its excellent electrochemical performance, due to the maintenance of the pitaya-like configuration during cycling. This structural stability guarantees the tight contact of Sb with carbon buffer as well as uniform distribution of Sb to balance the localized mechanical stress, so as to ensure excellent electrochemical performance. The structural design and synthetic method reported in this work may provide an effective way to stabilize the electrochemical performance of Na-storable alloy materials and therefore open a new prospect to create cycle-stable alloy anodes for high capacity Na-ion batteries.

Introduction

Sodium ion batteries (SIBs) are now considered as a key technologic solution to fulfill the cost-effective large scale electric energy storage, due to the wide abundance and ready availability of Na resources.[1-3] To realize SIB chemistry, a crucial issue is to discover applicable Na^+ host materials with sufficient lattice sites and channels available for Na^+ insertion reaction. Several classes of cathodic materials have been reported to show considerable Na storage capacities and cycling stability, including O3-$NaMO_2$,[4] P2-$Na_{0.67}MO_2$,[5-7] Honeycomb-layered $Na_3Ni_2SbO_6$,[8] transition-metal phosphates,[9-14] Orthorhombic $Na_{0.44}MnO_2$,[15] V_2O_5[16, 17, 18] and hexacyanoferrates,[19-22] and so on. This is in stark contrast to the situation in the search for suitable anode materials. Hard carbon materials are most extensively investigated for Na storage anode; however, these materials can only provide a usable capacity below 300 mAh g^{-1} and suffer from slow insertion kinetics and low volumetric energy density.[23-25]

A number of Na-storable metals and alloys have been recently revealed as high capacity anodes, such as Sn (847 mAh g^{-1}, $Na_{15}Sn_4$), Sb (660 mAh g^{-1}, Na_3Sb) Ge (1108 mAh g^{-1}, Na_3Ge) and Pb (484 mAh g^{-1}, $Na_{15}Pb_4$), etc.[26-28] However, the application of the alloy electrodes faces a great challenge of structural stability due to the drastic expansion/contraction during the Na alloying/dealloying, e. g. 525 % for Sn and 390 % for Sb.[29, 30] To address this problem, a facile approach is to develop nanosized materials integrated with conductive matrices that act as a buffer to accommodate the mechanical stress produced during the sodiation/desodiation reactions, prevent the particles aggregation as well as to provide electronic conduction. A series of reports have presented improved Na ion storage capacity and cycling stability of various nanostructured alloy anodes.[30-40] Xiao et al. firstly introduced a SbSn/C nanocomposite with a Na storage capacity of ~500 mAh g^{-1} and good cycling stability through the self-supporting of Sb and Sn.[30] Soon after, Qian et al. revealed a high-capacity and high-cycling Na-storage reaction on irregular Sb nanoparticles.[31] Other Sb-based nanocomposites were also reported to have a reversible capacity of ~600 mAh g^{-1} with good cycling performance.[34-37] Although these reports have tentatively confirmed that novel nanostructured designs can profoundly mitigate the large volumetric stress so as to improve the electrochemical performance of alloy materials, the relationship between the structural evolution and electrochemical performance during cycling is still far from well recognized.

Herein, we propose for the first time a novel pitaya-like Sb@C microsphere material used as Na ion storage anode. The microspherical architecture is compact and favors to obtain high tap density for practical applications. In the microspheres, electrochemically active Sb nanocrystallites with a diameter of 15~20 nm were uniformly distributed in the conductive carbon matrix. The material exhibits high reversible capacity, capacity retention as well as rate capability. Structural evolution characterization of the microspheres identifies that the pitaya-like Sb@C architecture is highly topological, which keeps the microenvironment of Sb nanocrystallites untouched during cycling. The findings gained here shed in-depth light on a strong dependence of the electrochemical performance on the microstructural stability.

Experimental

Samples preparation and characterization

The Sb@C microspheres were prepared using an aerosol spray

drying technique. The specific experiment was as following: 1.2 g polyacrylonitrile (PAN, Mw =150,000, Sigma-Aldrich Co. LLC.) and 12 g $SbCl_3$ (99 % purity, National Medicine Co., Ltd., China) were dissolved in 250 mL dimethylformamide (DMF) at 60 ^oC with vigorous stirring for 12 hour. The mixture was used for spray drying (SD-1500, Triowin Co., Ltd, China). The operating parameters were set as: in air = 170 ^oC, out air = 80 ^oC, disc rotation speed = 30,000 rpm, and the feed rate = ~ 300 mL/h. The collected particles were first heated at 280 ^oC for 6 h to consolidate their spherical morphology via the cyclization of PAN, and then heated at 700 ^oC for 6 h to obtain the Sb@C microspheres. The heating ramp was 2 ^oC min^{-1} and the atmosphere is Ar (92 vol. %) / H_2 (8 vol. %). The pure C microspheres were synthesized by using the above method without adding $SbCl_3$. Morphological characterizations of the Sb@C microspheres before and after sodiation were performed by a scanning electron microscopy (SEM, ULTRA/PLUS, ZEISS) and a transmission electron microscopy (TEM, JEOL, JEM-2010-FEF). The crystalline structures of the Sb@C microsphere were characterized by X-ray diffraction (XRD, Shimadzu XRD-6000). The composition analysis of the Sb@C microspheres was conducted with a thermogravimetric analyzer (Diamond TG/DTA 6300).

Electrochemical measurements

The Sb@C electrodes were prepared by mixing 80 wt% Sb@C microspheres, 10 wt% super P, and 10 wt% Polyacrylic acid (PAA, 25 wt%) to form a slurry, which was then coated onto a copper foil and dried at 60 ^oC overnight under vacuum. The charge/discharge performances of the electrodes were examined by 2016 coin-type cells by using a Sb@C electrode as the working electrode, a Na disk as the counter electrode, 1 M $NaPF_6$ dissolved in ethylene carbonate (EC)/diethyl carbonate (DEC) (1:1 by volume) with 5 % fluoroethylene carbonate (FEC) as the electrolyte, and a Celgard 2400 microporous membrane as the separator. All the cells were assembled in a glove box with water/oxygen content lower than 1 ppm and tested at room temperature. The galvanostatic charge/discharge test was conducted on a LAND cycler (Wuhan Kingnuo Electronic Co., China). The discharge/charge capacities of the Sb@C electrodes were calculated based on Sb in the composite by deducting the capacity contribution associated with carbon. Cyclic voltammetric measurements were carried out with the coin cells at a scan rate of 0.1 mV s^{-1} using a CHI 660 c electrochemical workstation (ChenHua Instruments Co., China).

Results and Discussion

Structural and morphological characterizations

The morphologic and structural features of the Sb@C microspheres were observed by SEM and TEM as shown in Figure 1. It shows that the sample appears as individual spheres with an average size of several micrometers (Figure 1a). A magnified image (Figure 1b) reveals that the surface of the microsphere looks very smooth and enwraps a large number of granules. The TEM image of a single microsphere (Figure 1c) shows a direct visual observation of a pitaya structure with the tiny seeds (Sb nanoparticles about 15~20 nm in diameters) uniformly embedded in the carbon matrix. This pitaya-like structure has a perfect dispersion of the active naonoparticles in the carbon buffer matrix, which should be expected to greatly accommodate the volume change during sodiation/desodiation processes, leading to a good cycling stability of the electrodes. Moreover, such dense microspheres could enable higher volumetric density than other nanoarchitectured Sb-C composites. The high-resolution TEM image in Figure 1d shows that the nanoparticles are highly crystalline as the spaces of the lattice fringes are visualized to be 0.225 nm, corresponding to the (104) plane of the hexagonal Sb (JCPDS No. 35-0732). The energy dispersive spectroscopy (EDS) mapping images also prove that Sb nanocrystallites are uniformly dispersed in the amorphous carbon matrix (Figure 1e and f).

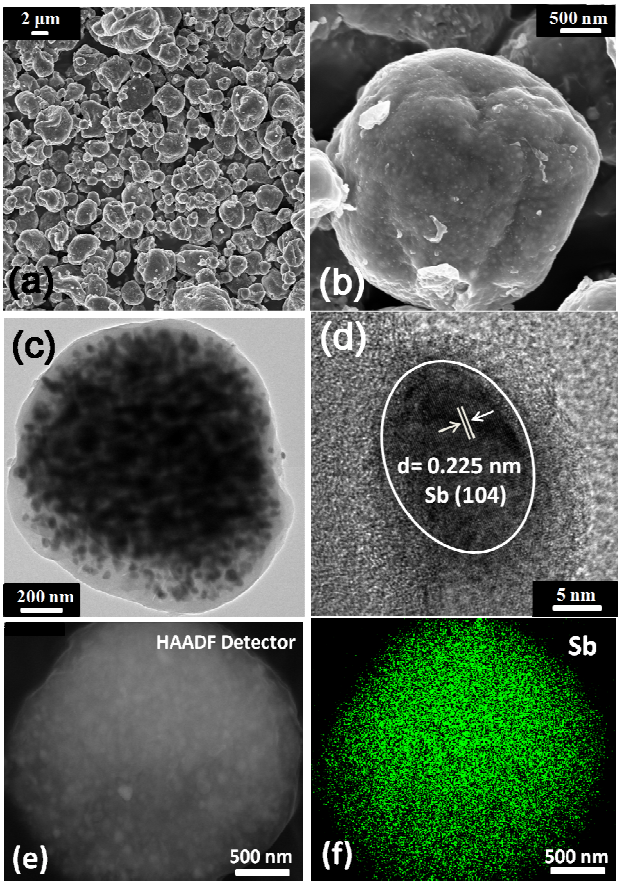

Figure 1 Morphological characteristics of the Sb@C microspheres: a) and b) SEM images. c) TEM image. d) High-resolution TEM image. e) SEM image for EDS analysis. f) Sb mapping image.

Electrochemical performances of Sb@C nanocomposite

Figure 2a shows the X-ray diffraction (XRD) patterns of the Sb@C microspheres. All of the diffraction reflections can be indexed to the hexagonal Sb (JCPDS No. 35-0732), suggesting high purity and crystallity of the Sb nanoparticles. The average size of Sb crystallites calculated from the FWHM of the (012) peak is about 20 nm, agreeing well with the direct observation from the TEM image in Figure 1. Obviously, small crystalline

sizes usually benefit to fast electrochemical reaction, high utilization of active materials as well as local strain release. The content of Sb in the Sb@C microspheres measured by TG analysis in air (Figure 2b) was found to be 40.8 %, assuming the final product was Sb_2O_4.[32]

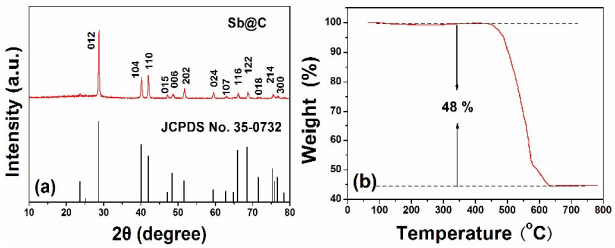

Figure 2 a) XRD pattern of the Sb@C microspheres. b) Thermogravimetric (TG) curve of the Sb@C microspheres in air.

Figure 3a shows the initial two cyclic voltammograms (CV) of the Sb@C microsphere electrode scanned between 0 and 2.0 V at a rate of 0.1 mV s^{-1}. The first negative scan shows no distinct reductive peaks until 0.08 V, indicating a high polarization during the first Na insertion into the large-sized Sb@C microspheres. The subsequent negative scan shows two reductive peaks appearing around at 0.43 and 0.32 V, which can be assigned to a two-step Na-Sb alloying reaction to form NaSb and Na_3Sb,[30] and another peak at 0.16 V due to the Na insertion into carbon.[22] The reversed positive scan presents one strong oxidative peak at 0.84 V and another shoulder peak at 0.96 V, characterizing the two-step Na-Sb dealloying reaction, and two weak oxidation peaks located at 0.30 and 0.61 V originated from the Na extraction from carbon. Therefore, the CV curves demonstrate that the Sb@C microsphere electrode can realize reversible sodiation/desodiation reaction at the potential region of 0 ~ 2.0 V (vs. Na^+/Na).

Figure 3b shows the initial two discharge/charge profiles of the Sb@C microsphere electrode cycled between 0.01 and 2.0 V at a current rate of C/15 (40 mA g^{-1}). The electrode presents a large potential polarization during the first discharge, similar to that observed in the CV plots. After the first activation process such as the electrolyte infiltration and structural rearrangement, the second discharge exhibits a distinct depolarization and a long potential plateau around 0.75 V and a short one at 0.57 V, in good accord with the charge plateaus at 0.78 and 0.89 V, representing a two-step Na-Sb alloying/dealloying process. The electrode delivers an initial charge (desodiation) capacity of 655 mAh g^{-1} calculated by deducting the capacity contribution from the PAN pyrolyzed carbon (~ 40 mAh g^{-1}, see Figure S1) and Supper P (90 mAh g^{-1}),[32] indicative of almost a full electrochemical utilization of Sb (the theoretical capacity is 660 mAh g^{-1}).

Figure 3c shows the cycling stability of the Sb@C microsphere electrode at a current rate of C/3 (200 mA g^{-1}). The electrode delivers an initial reversible capacity of 628 mAh g^{-1}. Over 100 cycles, the electrode still retains 93 % of the initial capacity. It should be noted that the coulombic efficiency of the Sb@C microsphere electrode is only 65 % during the first discharge/charge cycle. The high irreversible capacity loss should be mostly imputed to the decomposition of the electrolyte on the surface of the PAN pyrolyzed carbon in the microspheres, as it displays a very low initial coulombic efficiency of ~ 24 % (see Figure S1). However, the coulombic efficiency of the electrode rapidly increases to 95 % at the third cycle and then maintains higher than 99% afterwards, indicating that the electrolyte decomposition process only happens in the initial several cycles.

Figure 3d shows the rate cycling behavior of the Sb@C microsphere electrode manipulated from C/15 to 5 C. The electrode delivers a reversible capacity of 655, 637, 628, 600, 570 and 412 mAh g^{-1} at the current rates of C/15, C/6, C/3, 1C, 1.5 C and 3 C (1 C = 600 mA g^{-1}), respectively. Notably, as the current rate is as high as 5 C (3000 mA g^{-1}), the electrode still can deliver a high reversible capacity of 302 mAh g^{-1}, indicative of excellent rate capability. When the current rate is reset to C/3, the reversible capacity of the electrode rebounds to 622 mAh g^{-1}, approximate to the original capacity (628 mAh g^{-1}), showing high electrochemical reversibility of the Sb@C microsphere electrode for Na ion storage.

The above electrochemical characterization demonstrates that the Sb@C microspheres developed in this work has high reversible capacity, rate capability and cycling stability. The excellent electrochemical performances are preliminarily inferred to its unique pitaya-like configuration with the active Sb particles in ultrafine gain size (15~20 nm) highly dispersed in the pyrolyzed carbon matrix. The small crystalline size and tight contact with carbon is favorable for the full utilization of Sb and rapid Na ion insertion/extraction kinetics. In the meanwhile, this structural feature can greatly accommodate the mechanical stress as well as prevent the aggregation of the Sb nanoparticles during repeated Na insertion/extraction processes.

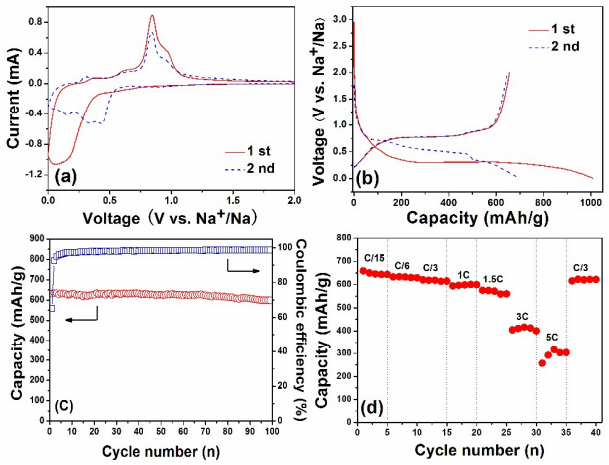

Figure 3 Electrochemical performance of the Sb@C microsphere electrodes. a) The initial two CV curves scanned between 0.01 and 2.0 V vs. Na^+/Na at a rate of 0.1 mV s^{-1}. b) The initial two discharge/charge profiles cycled at a current rate of C/15 (40 mA g^{-1}). c) The cycling performance at C/3 rate (200 mA g^{-1}). d) The rate cycling performance at various rates from C/15 to 5 C.

It is generally accepted that the structural robustness of materials determines their cycling ability, especially for alloy materials usually undergoing huge volumetric change during charge/discharge. The investigation of the structural evolution of the alloy electrodes during cycling should be very informative for identifying the structure-property dependence as well as guiding the structural design. Here, the structural evolution of the Sb@C microsphere electrodes during cycling is surveyed for the first time by SEM and TEM (Figure 4). Figure 4a and b show the SEM images of the Sb@C microsphere electrode after first

discharged to 0.01 V and recharged to 2.0 V, respectively. After the initial sodiation process (Figure 4a), the surface of the Sb@C microspheres become very rough compared to the fresh ones (Figure 1b), and many hemispheric protuberances are observed clearly, obviously arising from the volumetric expansion of the microspheres after anisotropic Na ion insertion. After the initial desodiation process, it is surprising to observe that dimensions of the microspheres are reverted to that of the original ones, and the surface of the microspheres is restored to its original smooth morphology (Figure 4b), indicating that the Sb@C microspheres are elastic enough to reversibly accommodate a huge volumetric expansion/shrinkage process. Figure 4c and d show the SEM images of the Sb@C microsphere electrode after the fifth discharge and charge. It is found that the original micron-sized spheres have been electrochemically grounded into many submicron spheres (500~700 nm in diameter). Upon continuous discharge/charge, it is found that the original microspheres are fully decomposed into botryoidal clusters and the sizes of the spheres become smaller (200-300 nm in diameter) after the 20th cycles (Figure 4e and f). At first glance of the morphologic evolution of the Sb@C microspheres during cycling, it looks that a pulverization process has occurred progressively, which may be

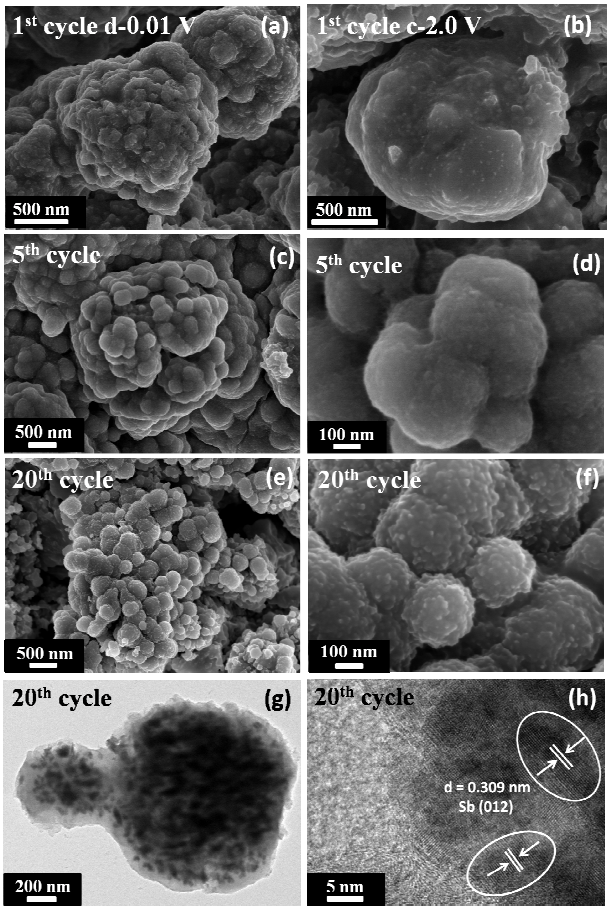

Figure 4 Morphological evolution of the Sb@C microspheres upon fully discharged to 0.01 V and charged to 2.0 V. a) and b) SEM images after the 1st discharge and charge. c) and d) SEM images after the 5th discharge and charge. e) and f) SEM images after the 20th discharge and charge. TEM image g) and high resolution TEM image h) after the 20th charge.

detrimental to the capacity retention of the electrodes. Of particular interest is the observation from the TEM images (Figure 4g and h), which shows the secondary submicrospheres still present a pitaya-like structure with Sb nanocrystallites uniformly embedded in the carbon phase (Figure 4g). Moreover, the size and crystallity of the Sb nanoparticles are almost unchanged (Figure 4h), indicating a full microstructural reversibility of Sb during the repeated phase transformations. The structural evolution of the Sb@C microspheres during cycling is schematically drawn in Figure 5.

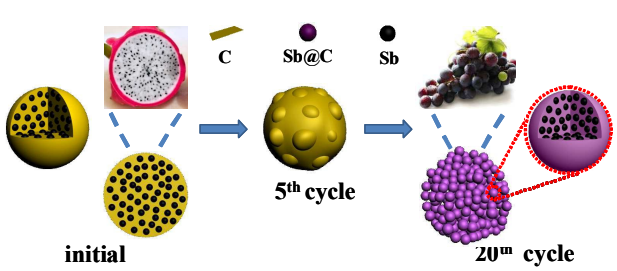

Figure 5 Schematic illustration for the structural evolution of the Sb@C microsphere upon cycling.

Overall, the chronology of the morphologic evolution of the Sb@C microspheres during cycling shows that a micron-sized pitaya structure is not elastic enough to bear the repeated mechanical expansion/contraction. However, the macro-pitaya structure maintains during the particulate degradation. More importantly, the micro-environment of Sb keeps untouched. These phenomena rather differ from those occurring on the bulk Sb or some Sb composites. As it is often observed that, during repeated expansion/contraction, a localized fracture of Sb happens, resulting in significant pulverization, amorphization, isolation or agglomeration to become electronically inactive. In contrast to the previous reports that Sb is permanently transformed into amorphous phase during one sodiation/desodiation process.[34] Sb particles can maintain full structural reversibility in this case. We believe that this structural reversibility mostly benefits from the topological pitaya structure and the small size of the Sb nanoparticles, which provides a strong buffer to greatly reduce the localized stress, or in other words, there is no microstructural evolution happening on this peculiar structure. These results reveal clearly that the electrochemical stability of the alloy materials is basically underlain on their microstructural robustness

Conclusions

In summary, we report a facile aerosol spray drying synthesis of pitaya-like Sb@C microspheres with ultrafine but well crystallized Sb nanoparticles uniformly dispersed in the carbon matrix. The Sb@C microsphere electrodes exhibit high Na storage capacity of 655 mAh g^{-1} at C/15 with excellent cyclability (93 % of capacity retention over 100 cycles) as well as remarkable rate capability. The morphological evolution of the Sb@C microspheres reveals the pitaya-like configuration persists upon cycling regardless of the macroscopic structural degradation. The topological structure guarantees the tight

contact of Sb with carbon buffer as well as uniform distribution to balance the localized mechanical stress, so as to ensure excellent electrochemical performance. Finally, the structural design and synthetic method reported in this work may provide an effective way to stabilize the electrochemical performance of Na-storable alloy materials and therefore open a new prospect to create cycle-stable alloy anodes for high capacity Na-ion batteries.

Acknowledgements

This work is financially supported by the National Basic Research Program of China (No. 2015CB251100), National Science Foundation of China (No. 21333007 and No. 21373155), Program for New Century Excellent Talents in University NCET-12-0419) and Hubei National Funds for Distinguished Young Scholars (2014CFA038).

Notes and references

a Hubei Key Lab. of Electrochemical Power Sources, College of Chemistry and Molecular Science, Wuhan University, China. E-mail: ylcao@whu.edu.cn;

b College of Chemistry, Central China Normal University, Wuhan 430079, China. E-mail: lfxiao@mail.ccnu.edu.cn.

1 H. Pan, Y.-S. Hu, L. Chen, *Energy Environ. Sci.* 2013, **6**, 2338.
2 B. L. Ellis, L. F. Nazar, *Curr. Opin. Solid State Mater. Sci.* 2012, **16**, 168.
3 M. D. Slater, D. Kim, E. Lee, C. S. Johnson, *Adv. Funct. Mater.* 2013, **23**, 947.
4 S.-M. Oh, S.-T. Myung, C. S. Yoon, J. Lu, J. Hassoun, B. Scrosati, K. Amine, Y.-K. Sun, *Nano Lett.* 2014, **14**, 1620.
5 D. Yuan, X. Hu, J. Qian, F. Pei, F. Wu, R. Mao, X. Ai, H. Yang, Y. Cao, *Electrochim. Acta* 2014, **116**, 300.
6 D. Yuan, W. He, F. Pei, F. Wu, Y. Wu, J. Qian, Y. Cao, X. Ai, H. Yang, *J. Mater. Chem. A* 2013, **1**, 3895.
7 N. Yabuuchi, M. Kajiyama, J. Iwatate, H. Nishikawa, S. Hitomi, R. Okuyama, R. Usui, Y. Yamada, S. Komaba, *Nat Mater.* 2012, **11**, 512.
8 D. Yuan, X. Liang, L. Wu, Y. Cao, X. Ai, J. Feng, H. Yang, *Advanced Materials* 2014, **26**, 6301.
9 Y. Liu, Y. Xu, X. Han, C. Pellegrinelli, Y. Zhu, H. Zhu, J. Wan, A. C. Chung, O. Vaaland, C. Wang, L. Hu, *Nano Lett.* 2012, **12**, 5664.
10 Y. Fang, L. Xiao, J. Qian, X. Ai, H. Yang, Y. Cao, *Nano Letters* 2014, **14**, 3539.
11 S.-M. Oh, S.-T. Myung, J. Hassoun, B. Scrosati, Y.-K. Sun, *Electrochem. Commun.* 2012, **22**, 149.
12 Z. Li, D. B. Ravnsbæk, K. Xiang, Y.-M. Chiang, *Electrochem. Commun.* 2014, **44**, 12.
13 Z. Jian, L. Zhao, H. Pan, Y.-S. Hu, H. Li, W. Chen, L. Chen, *Electrochem. Commun.* 2012, **14**, 86.
14 S. Li, Y. Dong, L. Xu, X. Xu, L. He, L. Mai, *Adv. Mater.* 2014, **26**, 3545.
15 Y. Cao, L. Xiao, W. Wang, D. Choi, Z. Nie, J. Yu, L. V. Saraf, Z. Yang, J. Liu, *Adv. Mater.* 2011, **23**, 3155.
16 V. Raju, J. Rains, C. Gates, W. Luo, X. Wang, W. F. Stickle, G. D. Stucky, X. Ji, *Nano Lett.* 2014, **14**, 4119.
17 D. W. Su, G. X. Wang, *ACS Nano* 2013, **7**, 11218.
18 D. W. Su, S. X. Dou, G. X. Wang, *J. Mater. Chem. A* 2014, **2**, 11185.
19 C. D. Wessells, R. A. Huggins, Y. Cui, *Nat Commun* 2011, **2**, 550.
20 C. D. Wessells, S. V. Peddada, R. A. Huggins, Y. Cui, *Nano Lett.* 2011, **11**, 5421.
21 J. Qian, M. Zhou, Y. Cao, X. Ai, H. Yang, *Adv. Energy Mater.* 2012, **2**, 410.
22 M. Pasta, C. D. Wessells, N. Liu, J. Nelson, M. T. McDowell, R. A. Huggins, M. F. Toney, Y. Cui, *Nat Commun* 2014, **5**, 3007.
23 Y. Cao, L. Xiao, M. L. Sushko, W. Wang, B. Schwenzer, J. Xiao, Z. Nie, L. V. Saraf, Z. Yang, J. Liu, *Nano Lett.* 2012, **12**, 3783.
24 S. Wenzel, T. Hara, J. Janek, P. Adelhelm, *Energy Environ. Sci.* 2011, **4**, 3342.
25 S. Komaba, W. Murata, T. Ishikawa, N. Yabuuchi, T. Ozeki, T. Nakayama, A. Ogata, K. Gotoh, K. Fujiwara, *Adv. Funct. Mater.* 2011, **21**, 3859.
26 V. L. Chevrier, G. Ceder, *J. Electrochem. Soc.* 2011, **158**, A1011.
27 C. Nithya, S. Gopukumar, *J. Mater. Chem. A* 2014, **2**, 10516.
28 D. Su, S. Dou, G. Wang, *Chem. Commun.* 2014, **50**, 4192.
29 C. Wang, Y. Xu, Q. Liu, Y. Zhu, Y. Liu, A. Langrock, M. R. Zachariah, *Nano Lett.* 2013.
30 L. Xiao, Y. Cao, J. Xiao, W. Wang, L. Kovarik, Z. Nie, J. Liu, *Chem. Commun.* 2012, **48**, 3321.
31 J. Qian, Y. Chen, L. Wu, Y. Cao, X. Ai, H. Yang, *Chem. Commun.* 2012, **48**, 7070.
32 L. Wu, X. Hu, J. Qian, F. Pei, F. Wu, R. Mao, X. Ai, H. Yang, Y. Cao, *Energy Environ. Sci.* 2014, **7**, 323.
33 D. Y. W. Yu, P. V. Prikhodchenko, C. W. Mason, S. K. Batabyal, J. Gun, S. Sladkevich, A. G. Medvedev, O. Lev, *Nat Commun* 2013, **4**.
34 A. Darwiche, C. Marino, M. T. Sougrati, B. Fraisse, L. Stievano, L. Monconduit, *J. Am. Chem. Soc.* 2012, **134**, 20805.
35 L. Wu, F. Pei, R. Mao, F. Wu, Y. Wu, J. Qian, Y. Cao, X. Ai, H. Yang, *Electrochim. Acta* 2013, **87**, 41.
36 Y. Zhu, X. Han, Y. Xu, Y. Liu, S. Zheng, K. Xu, L. Hu, C. Wang, *ACS Nano* 2013, **7**, 6378.
37 H. Zhu, Z. Jia, Y. Chen, N. Weadock, J. Wan, O. Vaaland, X. Han, T. Li, L. Hu, *Nano Lett.* 2013, **13**, 3093.
38 L. Wu, X. Hu, J. Qian, F. Pei, F. Wu, R. Mao, X. Ai, H. Yang, Y. Cao, *J. Mater. Chem. A* 2013, **1**, 7181.
39 J. Qian, Y. Xiong, Y. Cao, X. Ai, H. Yang, *Nano Lett.* 2014, **14**, 1865.
40 L. Wu, H. Lu, L. Xiao, J. Qian, X. Ai, H. Yang, Y. Cao, *J. Mater. Chem. A* 2014, **2**, 16424.

MS Title: Electrochemical Properties and Morphological Evolution of Pitaya-like Sb@C Microspheres as High-performance Anode for Sodium Ion Batteries

Authors: Lin Wu,[†] Haiyan Lu, Lifen Xiao,[*] Xinping Ai, Hanxi Yang, and Yuliang Cao[*]

Corresponding author: Yuliang Cao; College of chemistry and molecular science, Wuhan University, Wuhan 430072, China; E-mail: ylcao@whu.edu.cn

Graphical Abstract

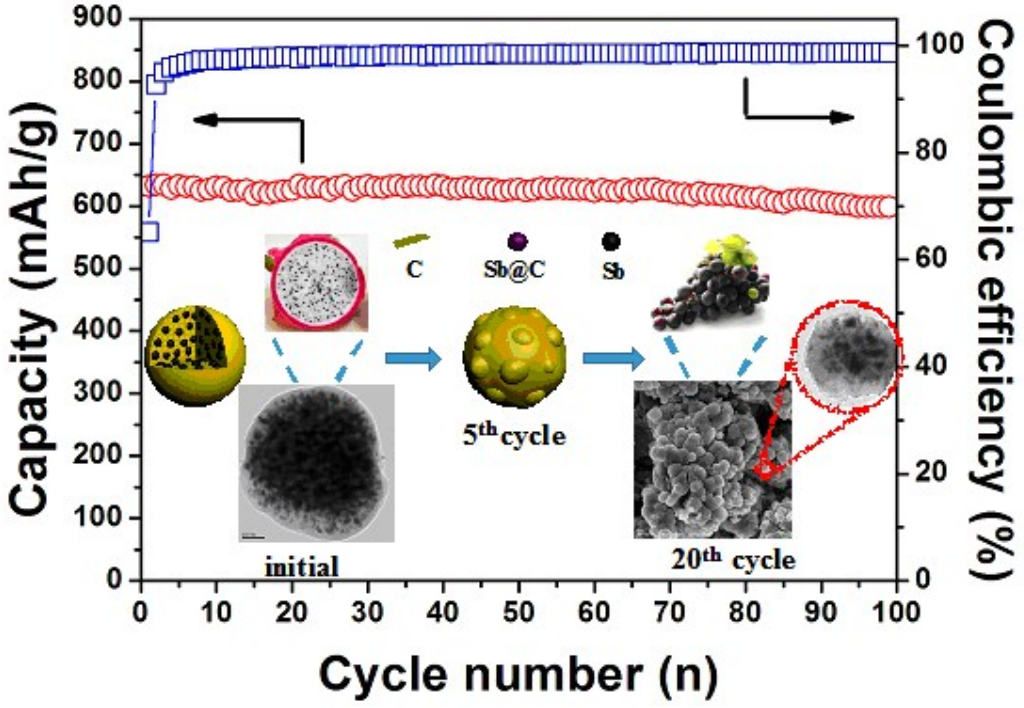

Pitaya-like Sb@C microspheres are prepared successfully via a facile aerosol spray drying method. The Sb@C microsphere anodes present a high initial capacity of 655 mAh g^{-1}, capacity retention of 93% over 100 cycles and high rate capability for Na-ion storage. The morphological evolution reveals the maintenance of the pitaya-like configuration guarantees the excellent electrochemical performance of the Sb@C microspheres.